OPEN ACCESS
Atmospheric Sciences ARTICLE

Enhanced influence of tropical Atlantic variability on East Asian summer monsoon in warming climate

Shangfeng Chen,[1,*] Wen Chen,[2,*] Renguang Wu,[3,*] Shang-Ping Xie,[4] Chunzai Wang,[5] Sang-Wook Yeh,[6] Zhibiao Wang,[1] Yuqiong Zheng,[2] and Linye Song[7]
*Correspondence: chenshangfeng@mail.iap.ac.cn (S.C.); chenwen-dq@ynu.edu.cn (W.C.); renguang@zju.edu.cn (R.W.)
Received: September 12, 2025; Accepted: March 3, 2026; Published Online: March 10, 2026; https://doi.org/10.59717/j.xinn-geo.2026.100207

The Innovation Geoscience

GRAPHICAL ABSTRACT

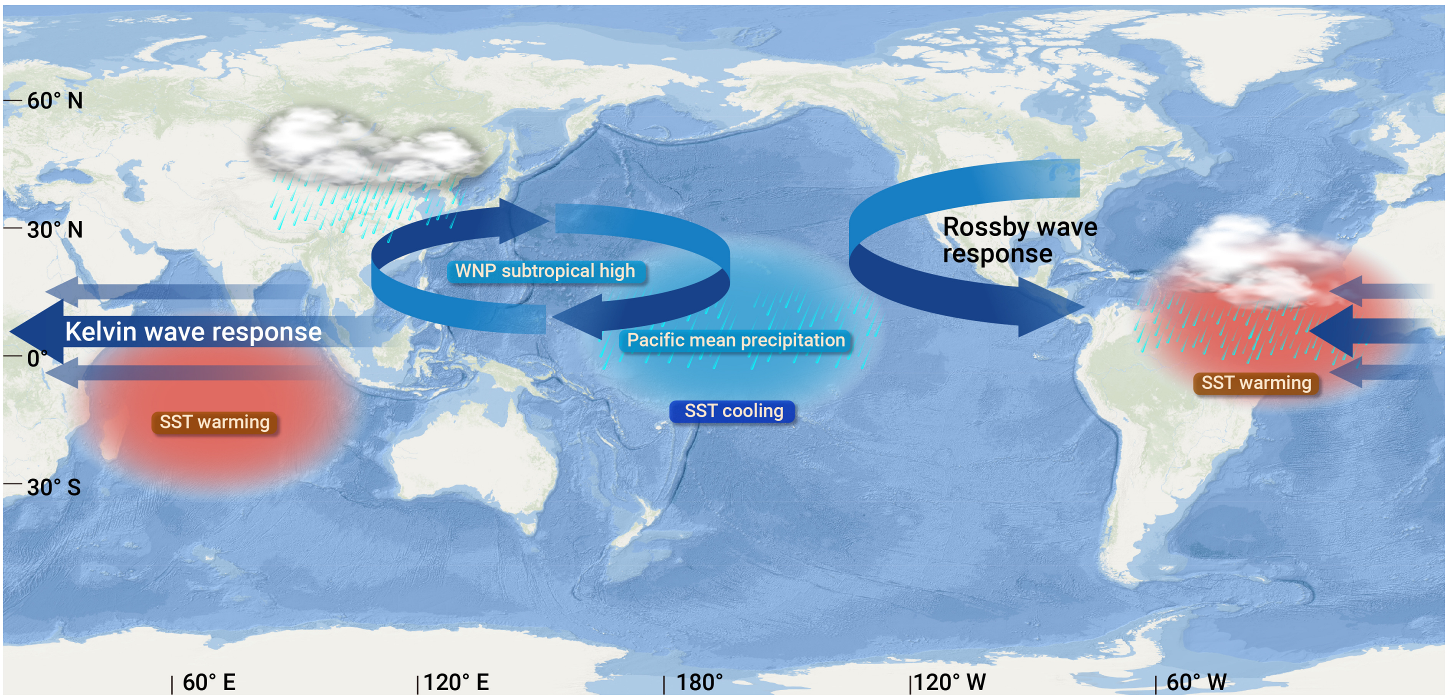

PUBLIC SUMMARY

- Spring North tropical Atlantic (SNTA) sea surface temperature (SST) variability enhances in a warming climate.
- Larger SNTA SST variability has greater impacts on East Asian Summer Monsoon (EASM) via Kelvin wave response.
- Wetter tropical Pacific in a warming climate also amplifies SNTA SST impact on EASM via Rossby wave response.

Enhanced influence of tropical Atlantic variability on East Asian summer monsoon in warming climate

Shangfeng Chen,[1,*] Wen Chen,[2,*] Renguang Wu,[3,*] Shang-Ping Xie,[4] Chunzai Wang,[5] Sang-Wook Yeh,[6] Zhibiao Wang,[1] Yuqiong Zheng,[2] and Linye Song[7]

[1]State Key Laboratory of Earth System Numerical Modeling and Application & Center for Monsoon System Research, Institute of Atmospheric Physics, Chinese Academy of Sciences, Beijing 100029, China

[2]Department of Atmospheric Sciences & Yunnan International Joint Laboratory of Monsoon and Climate Disasters, Yunnan University, Kunming 650500, China

[3]School of Earth Sciences, Zhejiang University, Hangzhou 310058, China

[4]Scripps Institute of Oceanography, University of California San Diego, La Jolla, CA 92093-0206, USA

[5]State Key Laboratory of Tropical Oceanography, South China Sea Institute of Oceanology, Chinese Academy of Sciences, Guangzhou 510301, China

[6]Department of Climate and Energy Systems Engineering, Ewha Womans University, Seoul 03760, South Korea

[7]Institute of Urban Meteorology, China Meteorological Administration, Beijing 100089, China

*Correspondence: chenshangfeng@mail.iap.ac.cn (S.C.); chenwen-dq@ynu.edu.cn (W.C.); renguang@zju.edu.cn (R.W.)

Received: September 12, 2025; Accepted: March 3, 2026; Published Online: March 10, 2026; https://doi.org/10.59717/j.xinn-geo.2026.100207

Citation: Chen S., Chen W., Wu R., et al. (2026). Enhanced influence of tropical Atlantic variability on East Asian summer monsoon in warming climate. *The Innovation Geoscience* **4**:100207.

The spring North tropical Atlantic (SNTA) sea surface temperature (SST) anomalies act as a critical precursor to the East Asian summer monsoon (EASM) and East Asian climate variability. However, how the influence of SNTA SST on the EASM changes in a warming climate remains unclear. Here, using multiple climate model simulations, we demonstrate a significant intensification of the impact of SNTA SST on EASM and East Asian climate under greenhouse warming. In a warmer climate, atmospheric and precipitation responses over East Asia to SNTA SST anomalies are remarkably amplified, contributing to a higher frequency of extreme EASM events following SNTA SST anomalies. Greenhouse warming increases SNTA SST variability, which enhances the response of tropical Indian Ocean SST anomalies via atmospheric teleconnection, thereby strengthening the impact on EASM through the stimulation of anomalous anticyclone over tropical western North Pacific. Meanwhile, a wetter tropical Pacific mean state in a warmer climate further amplifies the influence of SNTA SST-induced tropical central Pacific SST anomalies on the EASM. Our findings suggest that under continued greenhouse warming, the EASM will be increasingly modulated by SNTA SST, providing an opportunity to improve the predictability of East Asian climate.

INTRODUCTION

The East Asian summer monsoon (EASM) dominates weather and climate variations over East Asia and its surrounding regions.[1,2] Abnormal EASM variability often leads to extreme events, such as drought, flood, and heat wave events, which pose significant threats to food security, ecosystems, and human health.[2-4] For example, the strong EASM event in 2020 resulted in devastating floods in eastern China, causing hundreds of fatalities and tens of billions in economic losses.[5,6] Similar extreme EASM events in the summers of 1998 as well as 2016 also triggered catastrophic flooding throughout the Yangtze River basin, exerting pronounced influences on the ecosystem, agriculture and lives of people.[7,8] Given these substantial socioeconomic consequences, understanding the factors influencing EASM variability and improving its predictability are of paramount importance.

Tropical ocean conditions provide an important source of predictability for EASM and East Asian climate.[9-13] Sea surface temperature (SST) anomalies (SSTAs) associated with the El Niño-Southern Oscillation (ENSO) have marked impacts on EASM.[9-11] During the summer of El Niño decaying phase, equatorial central Pacific cold SSTAs generate an anomalous anticyclone over the tropical western north Pacific (TWNP) by triggering a westward-propagating cold Rossby wave.[9,10,14-17] This anomalous anticyclone strengthens the western Pacific subtropical high (WPSTH), which is a critical component of EASM,[9-11] resulting in increased precipitation over East Asia. Furthermore, warm SSTAs in the tropical Indian Ocean during El Niño decaying summer contributes to anticyclonic anomaly development over the TWNP by stimulating an atmospheric Kelvin wave.[11,12,16,17]

Emerging studies have suggested that spring north tropical Atlantic (SNTA) SSTAs has a remarkable influence on EASM independent of ENSO cycle.[18-23] SNTA SSTAs influence the tropical Pacific and Indian Ocean SST during the subsequent summer, which in turn affect EASM.[19,20] Observations show that many EASM events were coincided with preceding SNTA SSTAs, including strong EASM events in 1982, 1987, 1997, 2009, and 2019, as well as weak EASM events in 1993, 2007, 2011, and 2017 (Figure S1A). In addition, tropical Atlantic SSTAs provide a useful source for the prediction of East Asian climate.[24-27]

How the SNTA SSTAs forcing on the EASM may change in a warming climate? Studies found a marked enhancement for the relationship between SNTA SSTAs and EASM since the early1980s (Figure S1B).[28-30] Study indicated that the internal climate variability, e.g. the Interdecadal Pacific Oscillation, play a role in the recent enhanced impact of the tropical Atlantic SSTAs.[31] However, it remains unclear whether the intedecadal enhanced influence of SNTA SSTAs on EASM since the early 1980s can be entirely explained by internal climate variability or if it includes a contribution from greenhouse warming.[32,33] This study explores how the influence of SNTA SSTAs on EASM changes in a warmer climate via comparing two 91-year periods of simulations of 41 models from CMIP6. Our findings reveal that the influence of SNTA SSTAs on EASM is significantly enhanced under greenhouse warming. Hence, it is suggested that greenhouse warming has emerged as the one of the important factors driving the observed enhanced influence of SNTA SSTAs on the EASM since the early 1980s.

MATERIALS AND METHODS

Observational and reanalysis data

Monthly atmospheric data were provided by the National Centers for Environmental Prediction-National Center for Atmospheric Research reanalysis (NCEP-NCAR; https://www.esrl.noaa.gov/psd/data/gridded/data.ncep.reanalysis.derived.html).[34] SST data were extracted from the Extended Reconstructed Sea Surface Temperature dataset version 5 (https://psl.noaa.gov/data/gridded/data.noaa.ersst.v5.html).[35] Monthly precipitation data were derived from the Global Precipitation Climatology Project (https://psl.noaa.gov/data/gridded/data.gpcp.html).[36] The above observational data are all quadratically detrended in the respective full analysis period.

Model outputs from CMIP6

This study uses outputs from 41 coupled climate models participated in CMIP6 (Table S1; https://esgf-node.llnl.gov/projects/cmip6/). We use the historical simulations and the Shared Socioeconomic Pathway 5-8.5 scenario simulations (SSP85 simulations for short).[37] Monthly mean winds, geopotential height, surface temperature (employed to represent SST in the oceanic region) and precipitation rate data are all available for the historical simulations and SSP85 simulations from these 41 CMIP6 models. This study uses one realization from each model considering the model democracy.[38] Additionally, all outputs were quadratically detrended in the period of 1900-2100. In this study, present-day climate period is referred to the period over 1901-1991 (a total of 91-year) and future climate period is referred to the period over 2008-2098 (a total of 91-year).

Model experiments

We perform a series of AGCM simulations using CAM5 of the CESM model. Table S2 lists the details of the numerical simulations. EXP_{CTR} indicates the control simulation, which was run by observed monthly SST (termed EXP_{CTR}). The 1st sensitive simulation (denoted as EXP_{NTA1}) is similar to EXP_{CTR} except that additional monthly SSTAs are added from March to August in the tropical Atlantic (Figure S2 for the prescribed SSTAs). The 2nd sensitive simulation (termed EXP_{NTA2}) is similar to EXP_{NTA1} except that the amplitude of the prescribed SSTAs in the tropical Atlantic is two times of that in the EXP_{NTA1}. In the control and sensitive simulations, the models are integrated over 30 years. Note that only the last 20 model years in the simulations are employed for analysis.

In addition, to confirm the effect of the mean precipitation change in the enhanced impact of SNTA SSTAs, we have further run another two sets of simulations parallelly. First, a new control simulation termed EXP_{CTR_mean} is run, which is similar to the EXP_{CTR} but SST forcing in the tropical Pacific was set by a given JJA(0) mean SST (refer to Figure S3A for the prescribed forcing). The given mean SST has an amplitude of 1°C (Figure S3A). Adding the mean SST in the tropical Pacific to the AGCM simulation is an effective way of presenting the enhancement of mean precipitation in the tropical Pacific. The difference between EXP_{CTR_mean} and EXP_{CTR} shows stronger tropical Pacific precipitation (Figure S3B), verifying the reliability of this method. We then performed two sensitive simulations. The 1st sensitive simulation (termed EXP_{TCP}) is run by the observed SST plus prescribed JJA(0) SST cooling in the tropical Pacific (refer to Figure S3C for the prescribed SST). The second sensitivity simulation (termed EXP_{TCP_mean}) is similar to the EXP_{TCP} except that additional mean JJA(0) SST is added in the tropical Pacific. A comparison of the difference between EXP_{TCP} and EXP_{CTR} with the difference between EXP_{TCP_mean} and EXP_{CTR_mean} represents the influence of the mean precipitation.

Bootstrap test

We use bootstrap test method to check if the differences of the two quantities (e.g., SSTAs in the tropical Indian Ocean and tropical central Pacific related to the SNTA SST index) between 1901-1991 and 2008-2098 are significant.[39,40] Taking the JJA(0) SSTAs in the tropical Indian Ocean related to the SNTA index as an example, the JJA(0) SSTAs in the tropical Indian Ocean associated with the SNTA index are calculated via linear regression during 1901-1991 and 2008-2098 for the 41 models, seperately. Secondly, the JJA(0) SSTAs in the tropical Indian Ocean over 1901-1991 and 2008-2098 are randomly resampled to construct 10,000 samples. In this process, the JJA(0) SSTAs in the tropical Indian Ocean can be selected again in any models. If the MME difference of the JJA(0) SSTAs in the tropical Indian Ocean between 1901-1991 and 2008-2098 is greater compared to the sum of the standard deviations over 1901-1991 and 2008-2098, then the difference is significant at the 5% level.

EASM index

Following ref.[41], the EASM index (EASMI) is defined as the difference of the area-mean JJA(0) zonal wind at 850hPa between 22.5°-32.5°N, 110°-140°E and 5°-15°N, 90°-130°E. EASM index has been scaled to have one standard deviation over the entire analysis period to describe their temporal variations. To confirm the robustness of the obtained results, we also used two other methods with different variables to define the EASMI.[42,43] Specifically, ref.[42] defined EASMI as region-average 850hPa meridional wind over 20°-30°N and 110°-130°E, ref.[43] defined EASMI as the region-mean 850hPa vorticity over 10°-35°N and 100°-150°E.

SNTA index

SNTA index is defined as area-mean SSTAs in FMA(0) over 0°-15°N and 10°-65°W.[44] Slight changes in the region used to calculate SNTA index lead to similar results. SNAT index has been scaled to have one standard deviation over the entire analysis period to depict their temporal variations.

ENSO index

The Niño-3.4 SST index is employed to indicate the ENSO variability.

SNTA SSTAs events and anomalous EASM events

We use 1.0 standard deviation of the SNTA index as a criterion to identify SNTA SSTAs events and 1.0 standard deviation of the EASMI to define anomalous EASM events.

WPSTH index

The WPSTH index (WPSTHI) is defined according the previous study as region-mean 850-hPa stream function anomalies in JJA(0) (June-July-August-mean) over 5°-30°N and 115°-155°E.[14]

RESULTS

Connection between SNTA SST and EASM in observations and CMIP6 simulations

In the observations (Figure 1A), a stronger EASM is featured by a prominent anticyclonic anomaly over the TWNP, indicating an enhancement of the WPSTH (Figure 1A). The strengthening of the WPSTH leads to the transportation of much richer water vapor coming from the tropical regions towards East Asia, resulting in increased precipitation around the lower reaches of the Yangtze River, South Korea, and Japan (Figure S4A). At the same time, the enhanced WPSTH suppresses convection over the TWNP (Figure S4A). The ensemble mean (MME) of the 41 CMIP6 model simulations reproduces well the key features of the precipitation and atmospheric anomalies in association with the EASM (Figures 1C & S4B).

The atmospheric anomalies in association with the SNTA index (see Methods) are similar to those associated with the EASM (Figures 1A-B). Note that the anomalies related to the preceding winter Niño3.4 index have been linearly removed from the SNTA index (Methods) to ensure that the identified relationship is not due to the ENSO cycle.[28,29,44] The observed correlation coefficient during the period of 1979-2021 reaches 0.34 between the SNTA index and the EASM index (EASMI, Methods), which can pass the Pearson's significant test at the 5% level. In addition, the SNTA index shows a correlation coefficient of 0.38 with the JJA(0) WPSTH index (WPSTHI, Methods).

CMIP6 models simulate well the spring SST pattern in the northern tropical Atlantic during the historical period, as represented by the first leading mode of the FMA(0) SSTAs in the area of 0°-30°N and 0°-80°W.[45,46] The SNTA SST pattern in most CMIP6 models closely resembles the observations (Figures S5A-B), with the MME pattern correlation reaching 0.98 (Figure S5C). The observed close connections of the SNTA SST with the EASM and WPSTH can be well captured by the CMIP6 models in the historical period. A total of 34 CMIP6 models produce a positive correlation of the SNTA index with the EASMI and WPSTHI (Figures 1E-F). Furthermore, the observed correlation coefficient is the range of the CMIP6 ensemble (Figures 1E-F). Therefore, it is reasonable to use these models to investigate projected changes in the SNTA SST-EASM relationship in a warmer climate.

Enhanced forcing of SNTA SSTAs to EASM under greenhouse warming

The influence of SNTA SSTAs on the EASM shows an enhancement under greenhouse warming. The correlation between the SNTA index and the EASMI increases in 34 of the 41 CMIP6 models (approximately 82.9%) from the current climate period (1901-1991) to the future climate period (2008-2098) (Figure 2A). The MME correlation coefficient increases by 94%, from 0.16 during 1901-1991 to 0.31 during 2008-2098 (Figure 2A). This increase is significant at the 5% level according to the bootstrap test (Figures 2A & 3A, see bootstrap test in Methods). Note that different definitions of the EASM index yield similar results (Figures 2A & S6). Among the 34 CMIP6 models (excluding the 7 models that show a negative SNTA-EASM connection in the historical period, see Figure 1E), 28 models (about 82.4%) show an enhanced connection (Figure S7A), indicating a strong inter-model consensus. The relationship of SNTA index with JJA(0) WPSTHI also shows a significant increase in 34 of the 41 models in a warmer climate (Figure 2B). The MME correlation between SNTA index and WPSTHI increases by approximately 83%, from 0.18 during 1901-1991 to 0.33 during 2008-2098 (Figures 2B & 3B). Similarly, a strong inter-model consensus is found when considering only the 34 models, with 27 out of 34 models (approximately 79.4%) showing an enhanced connection of the SNTA SST anomalies with the WPSTH (Figure S7B).

The strengthened influences of SNTA SSTAs on the EASM and WPSTH are

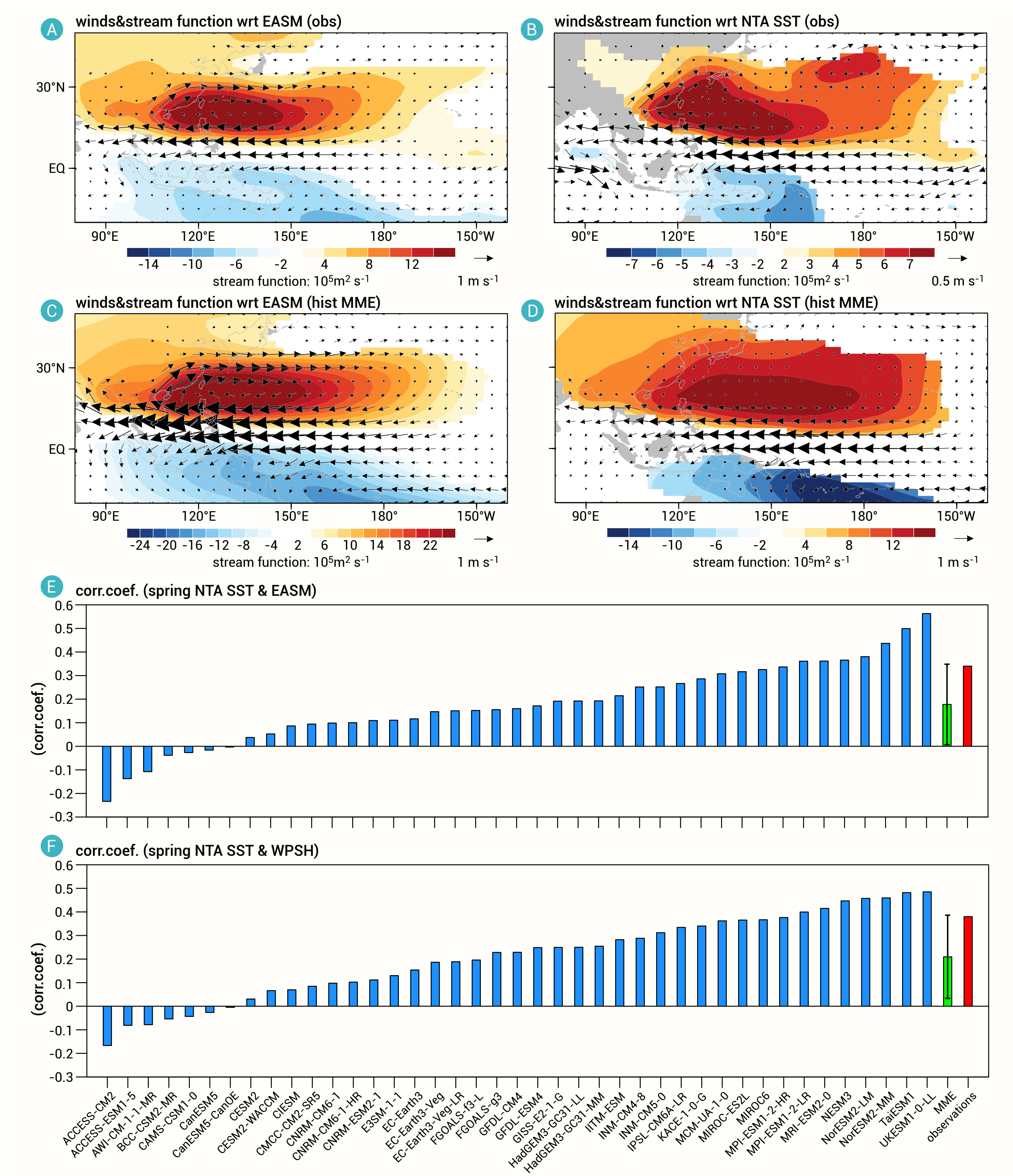

Figure 1. Relationship between SNTA SST and EASM in observations and CMIP6 models Anomalies of quadratically detrended JJA(0) 850-hPa winds and stream function regressed on the standardized (A) JJA(0) EASM index (see EASM index in Methods) and (B) SNTA SST index (see SNTA index in Methods) during 1979-2021 in observations. (C) and (D) are similar to (A) and (B), but for MME of 41 CMIP6 models during 1979-2014. Stream function anomalies that cannot pass the 95% confidence level in (A)-(D) are omitted. (E) Correlation coefficients between SNTA index and EASMI for the 41 CMIP6 models and their MME during 1979-2014. Error bar in (E) indicates one standard deviation of the correlation coefficients across the 41 models. Red bar in (E) indicates the observed result. (F) is similar to (E), but for the correlations between SNTA index and JJA(0) WPSTHI.

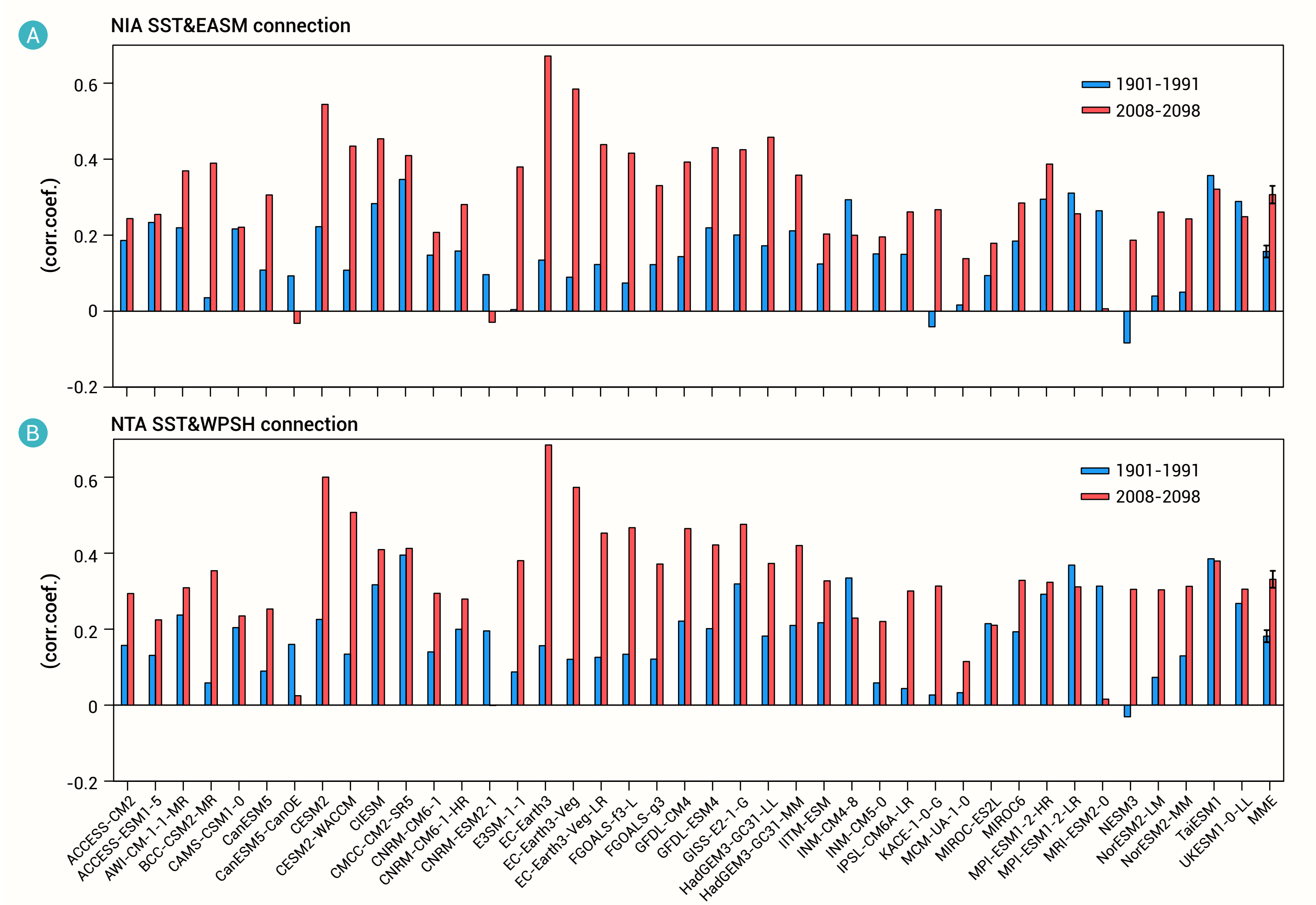

Figure 2. Enhanced influence of SNTA SST on EASM in a warmer climate (A) Correlations between SNTA index and EASMI during 1901-1991 and 2008-2098 for the 41 models and their MME. Error bar indicates one standard deviation of 10000 samples of the bootstrap test. (B) is similar to (A), but for the correlations between SNTA index and JJA(0) WPSTHI.

further confirmed by comparing JJA(0) atmospheric and precipitation anomalies related to the SNTA index between the periods 1901-1991 and 2008-2098 (Figures 3C-F). SNTA SST warming leads to a stronger anomalous anticyclone over TWNP (Figures 3C-D) and more pronounced precipitation responses over East Asia in the future climate (Figures 3E-F). Positive precipitation anomalies in JJA(0) over East Asia accompanied by SNTA index during 2008-2098 are approximately seven times larger than those during 1901-1991 (Figure S8).

There is a notable increase in the occurrence of anomalous EASM events on the heels of the SNTA SSTAs events (see Materials and Methods). The ratio of SNTA SST warming events followed by anomalously strong EASM events relative to the total SNTA SST warming events rises in 31 of the 41 models (75.6%) (Figure 4A), while the ratio of SNTA SST cooling events followed by anomalously weak EASM events increases in 26 of the 41 models (63.4%) under future warming climate (Figure 4B). Similarly, the occurrence ratios of SNTA SSTAs events followed by anomalous WPSTH events also show significant increases in the future warming climate (Figure S9). Thus, SNTA SSTAs exert a stronger influence on the EASM and contribute more significantly to the occurrence of extreme climate events over East Asia in a warmer climate.

Mechanism for enhanced impact of SNTA SSTAs on EASM

SNTA SSTAs influence the EASM by modulating the SST conditions in both tropical Indian Ocean and tropical central Pacific Ocean.[19,28,29,47] On one hand, SNTA SST warming causes surface easterly wind anomaly and SST warming over the tropical Indian Ocean through a Kelvin wave response.[19,48,49] The resulting tropical Indian Ocean warming further affects the WPSTH and EASM by triggering an anomalous anticyclone over the TWNP.[11,12,19] On the other hand, the SNTA warming leads to an anomalous cyclone over subtropical northeast Pacific through a Rossby wave response.[28,44] The northeasterly wind anomalies on the west side of this anomalous cyclone lead to tropical central Pacific SST cooling via bringing colder air from higher latitude regions and via increasing the evaporation by the enhanced wind speed via the WES feedback.[28,30,50] This SST cooling triggers an anomalous anticyclone over the TWNP by generating a cold Rossby wave to its west,[14,51,52] thereby contributing to an enhanced EASM.

SNTA SST variability is stronger during 2008-2098 than during 1901-1991 (Figure 5). The intensified SNTA SST variability in the future climate leads to a stronger atmospheric response in the tropical Indian Ocean (Figure S10), as reflected by the change in geopotential height anomalies in MAMJJA(0) over tropical Indian ocean (15°S-15°N and 50°-120°E) regressed on the SNTA index. The inter-model connection between the projected change of SNTA SST variability (2008-2098 minus 1901-1991) and the change of atmospheric response in the Indian Ocean is 0.68 across the 41 CMIP6 models, significant at the 1% level (Figure 6B). The enhanced atmospheric response results in a stronger SST response in the Indian Ocean (Figures 6C-D). The MME increase in JJA(0) Indian Ocean SST response to the SNTA SSTAs is 113%, rising from 0.10°C during 1901-1991 to 0.22°C during 2008-2098 (Figure S11). This stronger SST response in the tropical Indian Ocean leads to a greater impact on the EASM (Figures 6A & E).

The contribution of stronger SNTA SST variability to the amplified impact of SNTA SST on the EASM is verified by AGCM experiments (see Methods).[53] Three AGCM experiments are performed with one baseline control experiment (EXP_{CTR}) and another two sensitivity experiments (EXP_{NTA1} and EXP_{NTA2})

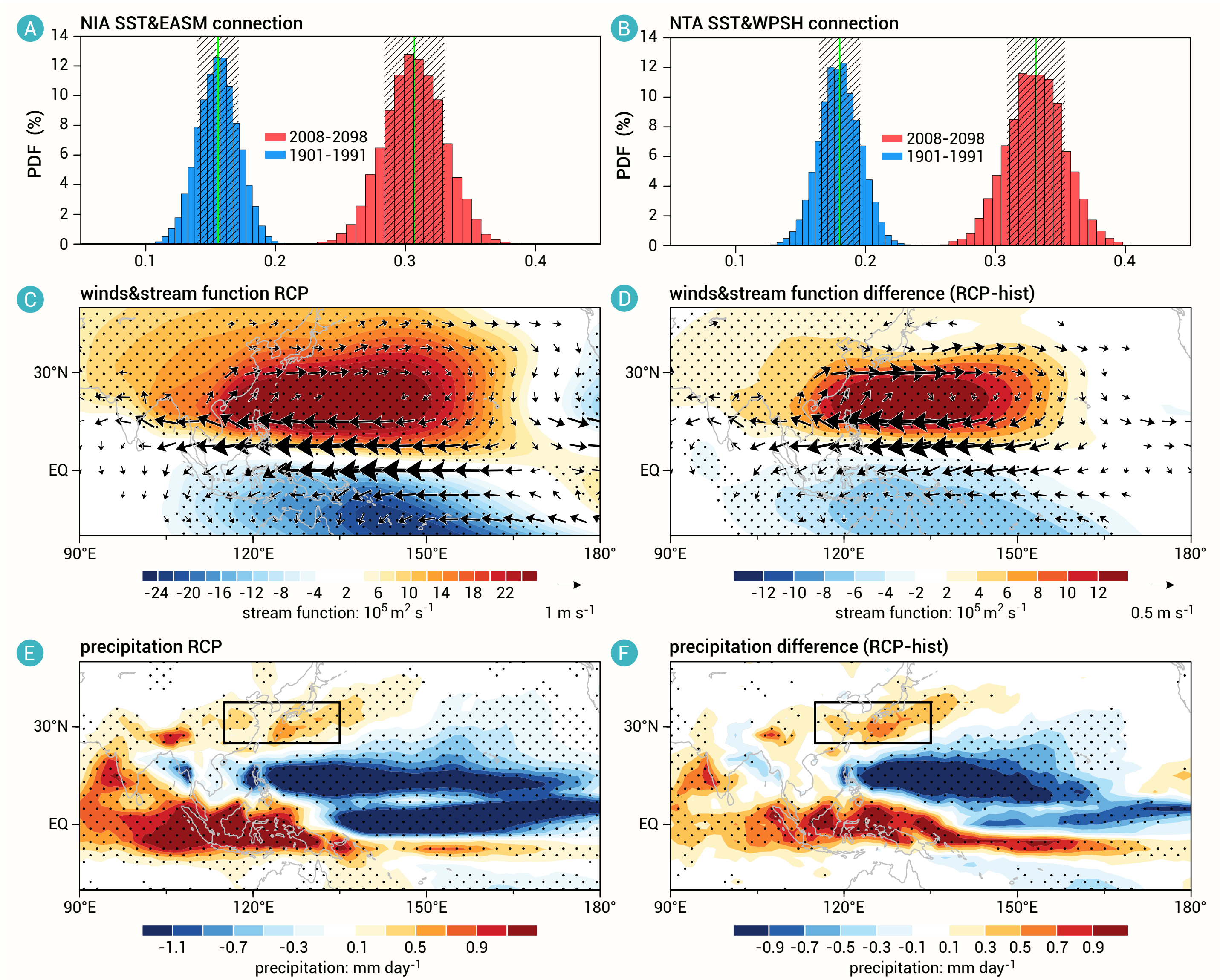

Figure 3. Enhanced influence of SNTA SST on East Asian climate in a warmer climate (A) Histograms of 10000 samples of a bootstrap test of the correlations between SNTA index and EASMI during 1901-1991 and during 2008-2098 for the 41 CMIP6 models. (B) is similar to (A), but for the correlation between SNTA index and JJA(0) WPSTHI. Green lines and stippling regions in (A)-(B) denote the mean value and standard deviation of the 10000 samples. Anomalies of quadratically detrended JJA(0) (C) 850-hPa winds and stream function, and (E) precipitation regressed on the standardized SNTA index for the CMIP6 MME during 2008-2098. Stippling regions in (C) and (E) indicate stream function and precipitation anomalies significant at the 95% confidence level. Differences in the JJA0 (D) 850-hPa winds and stream function, and (F) precipitation anomalies regressed on the standardized SNTA index between 2008-2098 and 1901-1991 for the CMIP6 MME. Stippling regions in (D) and (F) indicate differences in the stream function and precipitation anomalies significant at the 95% confidence level.

(see Table S2 and model experiments in Methods). In the EXP_{NTA2} experiment, the prescribed SST forcings in the NTA are two times of those in EXP_{NTA1} (Figure S2). Therefore, the difference between EXP_{NTA2} and EXP_{NTA1} indicates the role of the amplitude change in the SNTA SSTAs. A distinct anomalous cyclone is observed over subtropical northeast Pacific in MAMJJA(0) in the differences between EXP_{NTA1} and EXP_{CTR}, confirming the impact of SNTA SST warming through a Rossby wave (Figure 7A). Surface easterly surface wind anomalies are present over tropical Indian Ocean as a Kelvin wave response to the positive SNTA SSTAs (Figures 7A-B). Additionally, a strong anticyclonic anomaly occurs over TWNP, indicating an enhancement of the WPSTH. The EXP_{NTA2} experiment generates a significantly stronger atmospheric Kelvin wave response across the tropical Indian Ocean, marked by more pronounced low-level easterly wind anomalies (Figures 7A-B). Furthermore, the WPSTH response (defined as MAMJJA(0) 850-hPa stream function averaged over 5°-30°N, 115°-155°E) in EXP_{NTA2} is approximately twice as strong as in EXP_{NTA1} (Figure 7C). These model experiments confirm that stronger SNTA SST variability contributes to an enhanced impact on the EASM. Note that in these sensitive experiments, as only the NTA SSTAs are enhanced while the Indian Ocean SST and central Pacific SSTs are fixed, the impacts on the EASM are also evident. This suggests that the enhanced SNTA SSTAs can directly influence the EASM via the atmospheric processes, without involving the air-sea interaction and influencing the SSTAs in either the Indian Ocean or the tropical central Pacific.

SNTA SST warming leads to tropical central Pacific SST cooling in JJA(0) during both 1901-1991 and 2008-2098 (Figures S11B & D), with a slightly stronger amplitude in the future. However, the difference of the JJA(0) SST cooling in the tropical Pacific (5°S-5°N and 170°E-120°W) between 1901-1991 and 2008-2098 is not significant (Figure S12A). Furthermore, the inter-model relationships between the projected change in JJA(0) SST in the tropical central Pacific and the changes in SNTA SST variability, as well as the SNTA SST-EASM connection, are weak across the 41 CMIP6 models (Figures S12B-C). This indicates that the projected change in the influence of SNTA SSTAs on the EASM is not related to changes in the response of the tropical central Pacific to the preceding SNTA SSTAs.

Although the tropical Pacific SST responses in JJA(0) are comparable, mean precipitation in the tropical Pacific is much higher during 2008-2098 compared to that during the historical period (Figure S13).[54-56] The wetter mean state can lead to larger atmospheric anomalies in response to SST

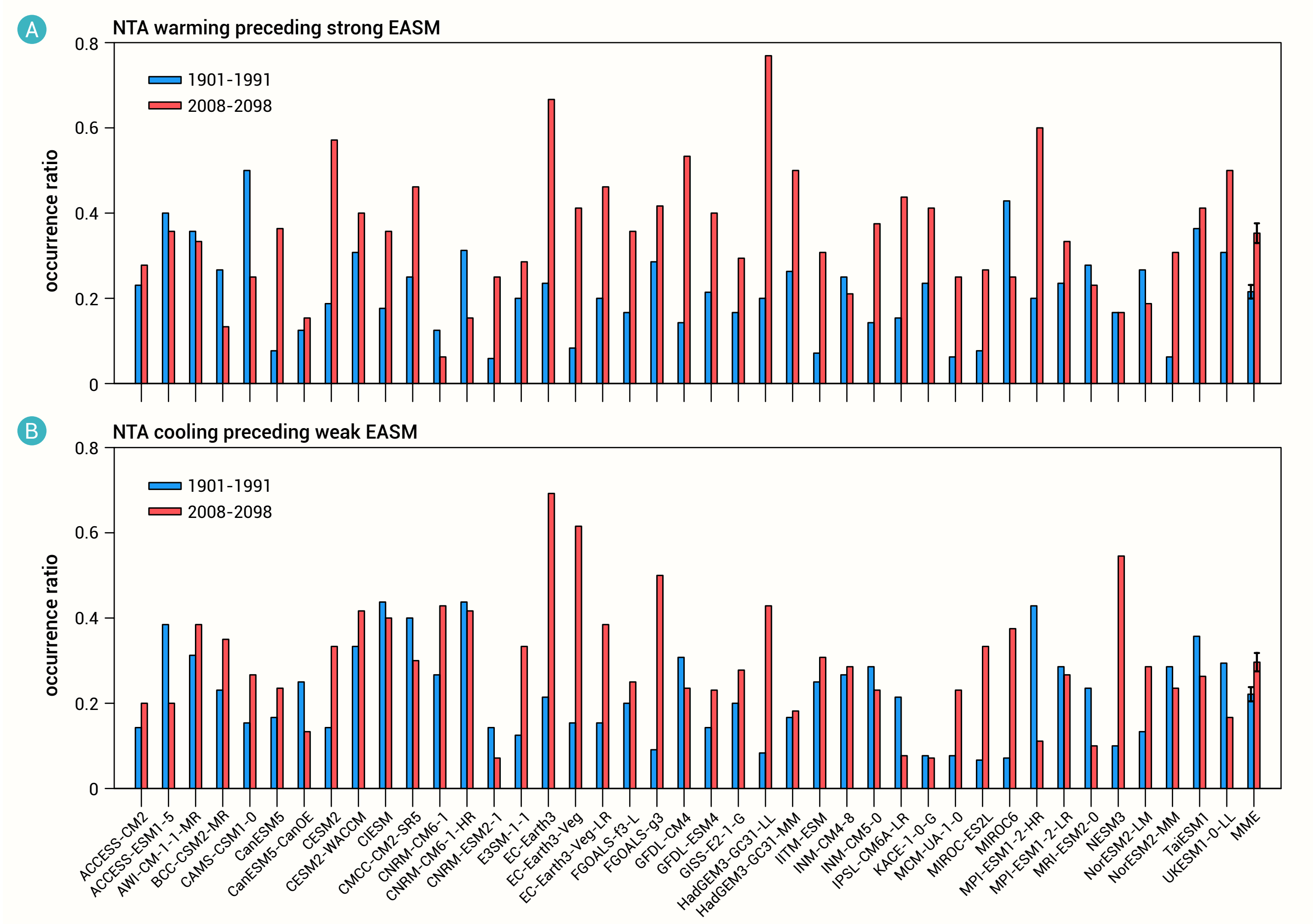

Figure 4. Increased frequency of SNTA SSTAs followed by anomalous EASM events under greenhouse warming Occurrence ratio of (A) SNTA SST warming followed by strong EASM events, and (B) SNTA SST cooling followed by weak EASM events during 1901-1991 and 2008-2098 for the 41 CMIP6 models. MME of the 41 models is shown, with error bars representing one standard deviation of 10000 samples of a bootstrap test.

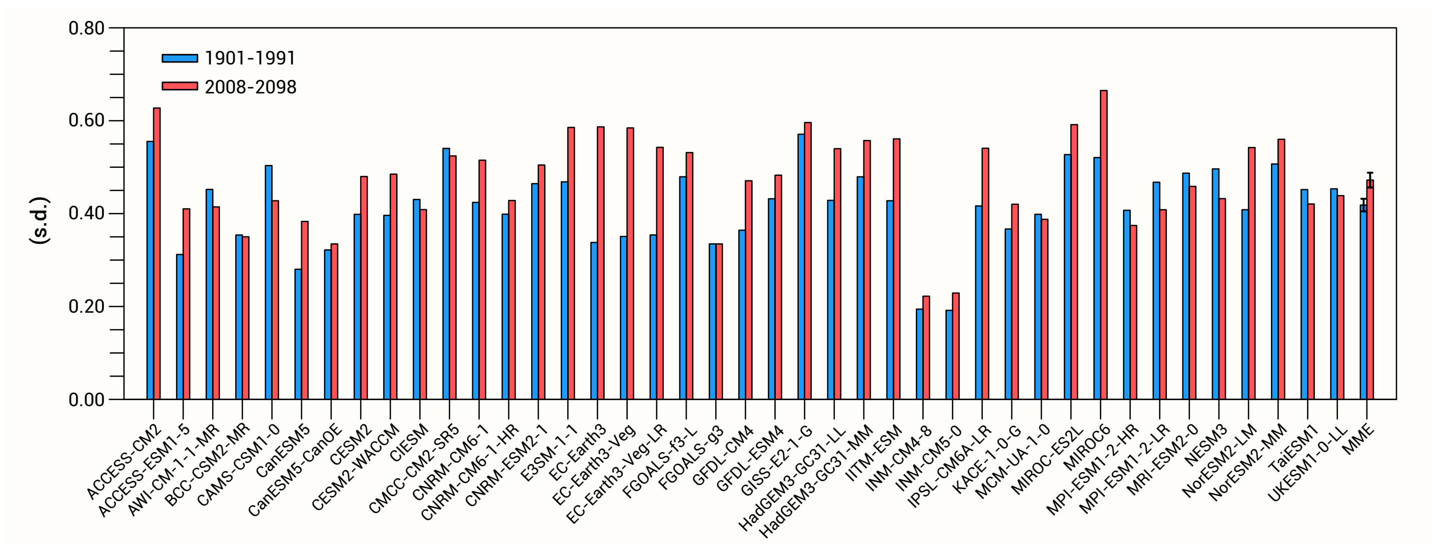

Figure 5. Enhanced SNTA SST variability in a warmer climate Standard deviation of SNTA index during 1901-1991 and 2008-2098 for the 41 models and their MME.

changes of the same magnitude.[57-58] The inter-model connection between the projected change in the precipitation climatology in the equatorial central Pacific (2.5°S-2.5°N, 180°-110°W) and the change in the SNTA SST-EASM connection reaches 0.7 across the 41 CMIP6 models (Figure 6F). This suggests that the wetter mean state in the tropical Pacific under warmer climate can contribute to an enhanced forcing of SNTA SSTAs to the EASM.

To confirm the contribution of mean precipitation change to the enhanced impact of SNTA SST, we conducted two additional sets of simulations (i.e. EXP_{TCP_mean} and EXP_{CTR_mean}, EXP_{TCP} and EXP_{CTR}) (see Table S2 and model experiments in Methods). A comparison of the difference between EXP_{TCP}

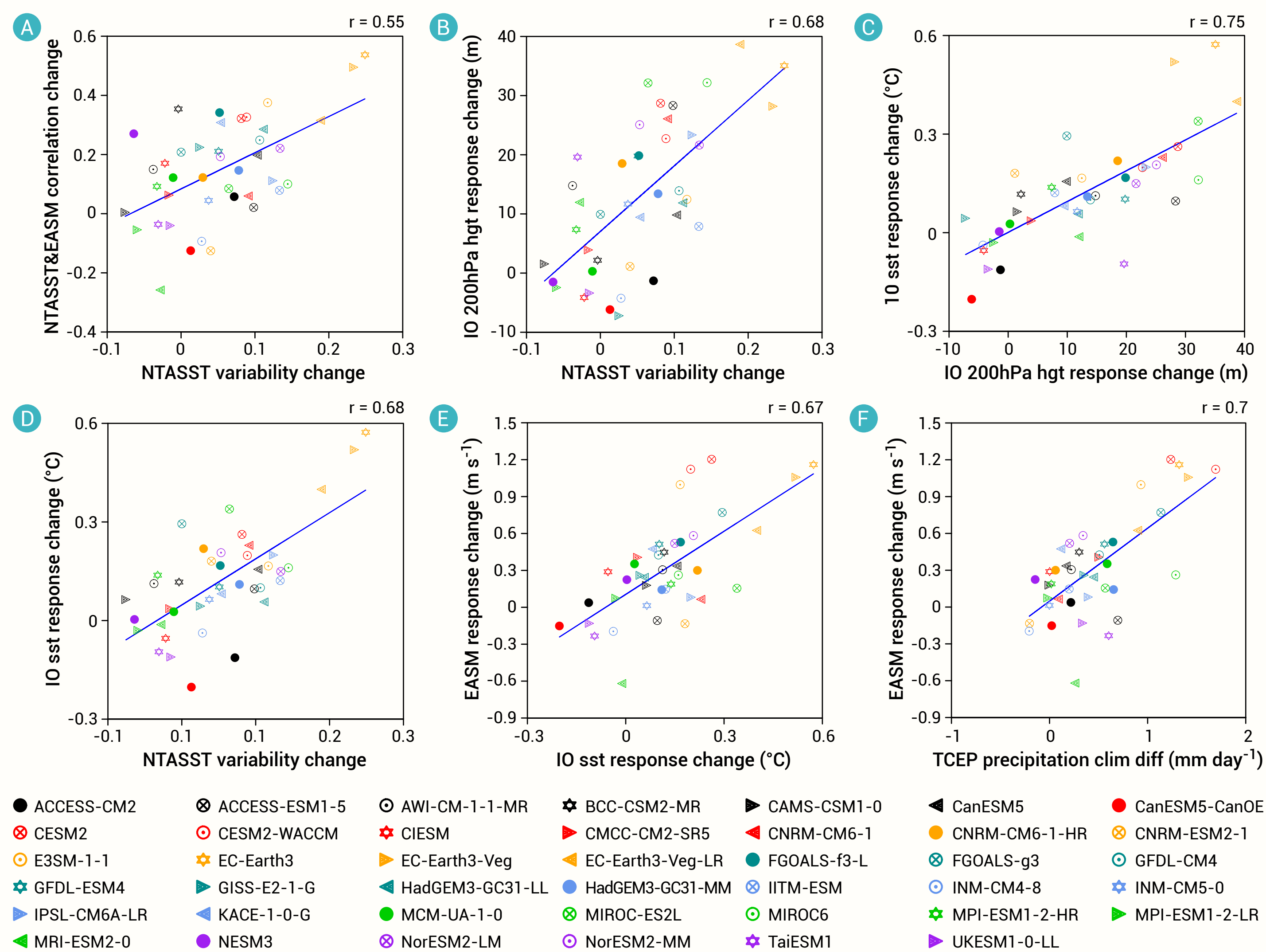

Figure 6. Mechanisms for enhanced impact of SNTA SST on EASM in a warmer climate Inter-model relationships between projected change in SNTA SST variability against (A) change in the correlation between SNTA index and EASMI, and against (B) change in the FMA(0) 200-hPa geopotential height over the tropical Indian Ocean (IO, 15°S-15°N and 50°-120°E) responses to SNTA SST, and against (D) change in the JJA(0) SST in the tropical IO responses to SNTA SST across the 41 CMIP6 models. (C) Inter-model connection between projected change in the FMA(0) 200-hPa geopotential height over the tropical IO responses to SNTA SST against change in the JJA(0) SST in the tropical IO responses to SNTA SST. Inter-model relationships between projected change in the EASM responses to SNTA SST against (E) change in the JJA(0) SST in the tropical IO responses to SNTA SST, and against (F) change in the MAMJJA(0) precipitation climatology in the tropical central Pacific.

and EXP_{CTR} with the difference between EXP_{TCP_mean} and EXP_{CTR_mean} represents the role of the mean precipitation change. The differences between the EXP_{TCP} and EXP_{CTR} indicate that SST cooling in the tropical central Pacific leads to an anticyclonic anomaly over the TWNP through a Rossby wave, which then further impacts EASM (Figures 7D-E). In comparison, the anticyclonic anomaly over the TWNP is significantly stronger in the difference between EXP_{TCP_mean} and EXP_{CTR_mean} than that between EXP_{TCP} and EXP_{CTR}. In particular, the JJA(0) WPSTH response (defined as JJA(0) 850-hPa stream function averaged over 5°-30°N, 115°-155°E) in the EXP_{TCP_mean} is more than two times larger than that in the EXP_{TCP} (Figure 7F). These numerical experiments verify that wetter mean state in the tropical Pacific under future warming climate leads to a stronger atmospheric response to the same SSTAs in the tropical central Pacific.

DISCUSSION AND CONCLUSION

This study reveals that the influence of SNTA SSTAs on EASM becomes stronger in a warmer climate. In the future, with a warmer climate, SNTA SST variability increases, resulting in stronger atmospheric and SST responses in the tropical Indian Ocean. This, in turn, leads to stronger tropical Indian Ocean SSTAs, which further amplify its impact on the EASM through an atmospheric Kelvin wave response. Meanwhile, tropical central Pacific SSTAs in summer, generated by the preceding SNTA SST variation, remain comparable in both present-day and future climates. However, a wetter mean state in the tropical Pacific under future warming climate leads to a much stronger impact on the EASM through an atmospheric Rossby wave response. The mechanisms responsible for the enhanced impact of SNTA SSTAs on the following EASM are confirmed through numerical experiments. The present study indicates that SNTA SSTAs have become an increasingly more influential factor for the EASM variation as greenhouse warming continues, thereby potentially improving the prediction skill of EASM and East Asian climate.

Recent study suggested that the increase in the interannual variability of SST in the northern tropical Atlantic under greenhouse warming may be linked to the enhanced influence of the preceding winter ENSO via atmospheric teleconnection.[59] In the present study, the impact of the preceding winter ENSO has been excluded. Beyond ENSO, other factors also significantly contribute to SNTA SST variability, such as the North Atlantic Oscillation and air-sea interactions in the tropical Atlantic.[45,60,61] Further investigations will be carried out to explore the relative roles of the NAO and air-sea interactions in the projected change of SNTA SST variability. In addition, studies suggested that in the higher-resolution model experiment, the EASM simulation is much improved.[62] In the future, we would that use this high-resolution air-sea coupled models to further investigate the SNTA SST-EASM relationship.

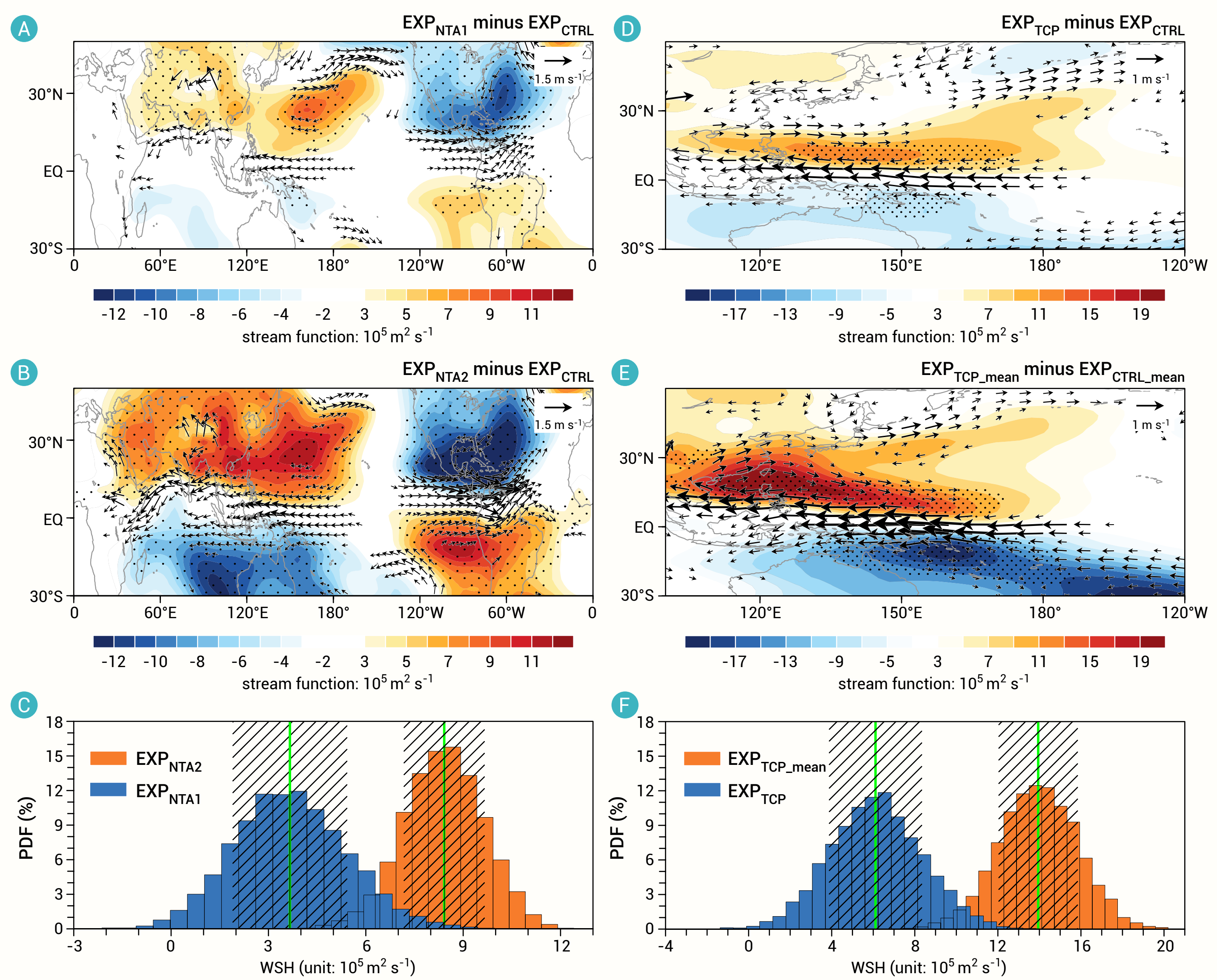

Figure 7. Numerical experiments confirming enhanced impact of SNTA SSTAs on EASM due to increased NTA SST variability and wetter mean state in tropical Pacific Differences of MAMJJA(0) 850-hPa winds and stream function between (A) EXP_{NTA1} and EXP_{CTR}, and (B) between EXP_{NTA2} and EXP_{CTR}. (C) Histograms of 10000 samples for the differences in region-mean MAMJJA(0) 850-hPa stream function over 5°-30°N, 115°-155°E between EXP_{NTA1} and EXP_{CTR} (blue bar), and (B) between EXP_{NTA2} and EXP_{CTR} (red bar). Differences of JJA(0) 850-hPa winds and stream function between (D) EXP_{TCP} and EXP_{CTR}, and (E) between $EXP_{TCP\_SSTclim}$ and $EXP_{CTR\_SSTclim}$ (see model experiments in Methods). (F) Histograms of 10000 samples for the differences in region-mean JJA(0) 850-hPa stream function over 5°-30°N, 115°-155°E between EXP_{TCP} and EXP_{CTR} (blue bar), and (B) between $EXP_{TCP\_SSTclim}$ and $EXP_{CTR\_SSTclim}$ (red bar). Stippling regions in (A)-(B) and (D)-(E) indicate differences of the stream function significant at the 95% confidence level. Green lines and stippling regions in (C) and (F) denote the mean value and the standard deviation.

REFERENCES

1. Tao S. and Chen L. (1987). A review of recent research on the East Asian summer monsoon in China. Chang C.-P. and Krishnamurti T.N. (eds). *Monsoon Meteorology* (Oxford Univ. Press), pp:60–92. https://www.researchgate.net/publication/266375342_A_Review_of_Recent_Research_on_the_East_Asian_Summer_Monsoon_in_China
2. Ding Y.-H. and Chan J.C.L. (2005). The East Asian summer monsoon: An overview. *Meteor. Atmos. Phys.* 89:117–142. DOI:10.1007/s00703-005-0125-z
3. Ha K.-J., Heo K.-Y., Lee S.-S., et al. (2012). Variability in the East Asian Monsoon: A review. *Meteorol. Appl.* 19:200–215. DOI:10.1002/met.1320
4. Zhang Q., Zheng Y., Singh V.P., et al. (2017). Summer extreme precipitation in eastern China: Mechanisms and impacts. *J. Geophys. Res.* 122:2766–2778. DOI:10.1002/2016JD025913
5. Liang P., Hu Z., Ding Y., et al. (2021). The extreme Mei-Yu season in 2020: Role of the Madden-Julian oscillation and the cooperative influence of the Pacific and Indian Oceans. *Adv. Atmos. Sci.* 38:2040–2054. DOI:10.1007/s00376-021-1078-y
6. Zhou Z.-Q., Xie S.-P. and Zhang R.-H. (2021). Historic Yangtze flooding of 2020 tied to extreme Indian Ocean conditions. *Proc. Natl. Acad. Sci. USA* 118:e2022255118. DOI:10.1073/pnas.2022255118
7. Lau K. and Weng H. (2001). Coherent modes of global SST and summer rainfall over China: An assessment of the regional impacts of the 1997–98 El Niño. *J. Clim.* 14:1294–1308. DOI:10.1175/1520-0442(2001)014<1294:CMOGSA>2.0.CO;2
8. Zhai P., Yu R., Guo Y., et al. (2016). The strong El Niño of 2015/16 and its dominant impacts on global and China's climate. *J. Meteor. Res.* 30:283–297. DOI:10.1007/s13351-016-6101-3
9. Zhang R.-H., Sumi A. and Kimoto M. (1996). Impact of El Nino on the East Asian monsoon: A diagnostic study of the 86/87 and 91/92 events. *J. Meteor. Soc. Jap.* 74:49–62. DOI:10.2151/jmsj1965.74.1_49
10. Wang B., Wu R. and Fu X. (2000). Pacific–East Asian teleconnection: How does ENSO affect East Asian climate. *J. Clim.* 13:1517–1536. DOI:10.1175/1520-0442(2000)013<1517:PEATHD>2.0.CO;2
11. Xie S.-P., Hu K.-M., Hafner J., et al. (2009). Indian Ocean capacitor effect on Indo–Western Pacific climate during the summer following El Niño. *J. Clim.* 22:730–747. DOI:10.1175/2008JCLI2544.1
12. Xie S.-P., Kosaka Y., Du Y., et al. (2016). Indo-western Pacific ocean capacitor and coherent climate anomalies in post-ENSO summer: A review. *Adv. Atmos. Sci.* 33:411–432. DOI:10.1007/s00376-015-5192-6
13. Zhang P.-C., Xie S.-P., Kosaka Y., et al. (2024). Why East Asian monsoon anomalies are more robust in post El Niño than in post La Niña summers. *Nat. Commun.* 15:7401. DOI:10.1038/s41467-024-51885-7

14. Yang K., Cai W.-J., Huang G., et al. (2022). Increased variability of the western Pacific subtropical high under greenhouse warming. *Proc. Natl. Acad. Sci. USA* **119**:e2120335119. DOI:10.1073/pnas.2120335119
15. Wang C.-Y., Zheng X.-T. and Xie S.-P. (2023). Enhanced ENSO-unrelated summer variability in the Indo-western Pacific under global warming. *J. Clim.* **36**:1749–1765. DOI:10.1175/JCLI-D-22-0450.1
16. Song F. and Zhou T. (2014). The climatology and inter-annual variability of East Asian summer monsoon in CMIP5 coupled models: Does air-sea coupling improve the simulations. *J. Clim.* **27**:8761–8777. DOI:10.1175/JCLI-D-14-00396.1
17. Song F. and Zhou T. (2014). Inter-annual variability of East Asian summer monsoon simulated by CMIP3 and CMIP5 AGCMs: Skill dependence on Indian Ocean-western Pacific anticyclone teleconnection. *J. Clim.* **27**:1679–1697. DOI:10.1175/JCLI-D-13-00248.1
18. Lu Z., Dong L., Song F., et al. (2024). Quantifying the relative contributions of three tropical oceans to the western North Pacific anomalous anticyclone. *Environ. Res. Lett.* **19**:104016. DOI:10.1088/1748-9326/ad677d
19. Rong X.Y., Zhang R.H. and Li T. (2010). Impacts of Atlantic sea surface temperature anomalies on Indo-East Asian summer monsoon-ENSO relationship. *Chin. Sci. Bull.* **55**:2458–2468. DOI:10.1007/s11434-010-3098-3
20. Hong C.-C., Lee M.-Y., Hsu H.-H., et al. (2014). Tropical SST forcing on the anomalous WNP subtropical high during July–August 2010 and the record-high SST in the tropical Atlantic. *Clim. Dyn.* **45**:633–650. DOI:10.1007/s00382-014-2275-5
21. Wang C.-Z. (2006). An overlooked feature of tropical climate: Inter-Pacific-Atlantic variability. *Geophys. Res. Lett.* **33**:L12702. DOI:10.1029/2006GL026324
22. Wang C.-Z. (2019). Three-ocean interactions and climate variability: A review and perspective. *Clim. Dyn.* **53**:5119–5136. DOI:10.1007/s00382-019-04930-x
23. Jin D.-C. and Huo L.-W. (2018). Influence of tropical Atlantic sea surface temperature anomalies on the East Asian summer monsoon. *Quart. J. Roy. Meteor. Soc.* **144**:1490–1500. DOI:10.1002/qj.3296
24. Keenlyside N.S., Ding H. and Latif M. (2013). Potential of equatorial Atlantic variability to enhance El Niño prediction. *Geophys. Res. Lett.* **40**:2278–2283. DOI:10.1002/grl.50362
25. Martín-Rey M., Rodríguez-Fonseca B. and Polo I. (2015). Atlantic opportunities for ENSO prediction. *Geophys. Res. Lett.* **42**:6802–6810. DOI:10.1002/2015GL065062
26. Chikamoto Y., Timmermann A., Luo J., et al. (2015). Skillful multi-year predictions of tropical trans-basin climate variability. *Nat. Commun.* **6**:6869. DOI:10.1038/ncomms7869
27. Liang P. and Lin H. (2018). Sub-seasonal prediction over East Asia during boreal summer using the ECCC monthly forecasting system. *Clim. Dyn.* **50**:1007–1022. DOI:10.1007/s00382-017-3658-1
28. Hong C.-C., Chang T.-C. and Hsu H.-H. (2014). Enhanced relationship between the tropical Atlantic SST and the summertime western North Pacific subtropical high after the early 1980s. *J. Geophys. Res.* **119**:3715–3722. DOI:10.1002/2013JD021394
29. Chang T., Hsu H.-H. and Hong C. (2016). Enhanced influences of tropical Atlantic SST on WNP–NIO atmosphere–ocean coupling since the early 1980s. *J. Clim.* **29**:6509–6525. DOI:10.1175/JCLI-D-15-0807.1
30. Jin D.-C., Huo L.-W., Yan Z., et al. (2024). Enhanced influence of tropical Atlantic Sea surface temperature anomalies on east Asian summer monsoon since the late 1970s. *Clim. Dyn.* **62**:5745–5757. DOI:10.1007/s00382-024-07173-7
31. Wang H., Li Z., Li J.-P., et al. (2023). Interannual variation in the East Asian summer monsoon-tropical Atlantic SST relationship modulated by the Interdecadal Pacific Oscillation. *npj Clim. Atmos. Sci.* **6**:169. DOI:10.1038/s41612-023-00497-x
32. Wallace J.M., Deser C., Smoliak B.V., et al. (2013). Attribution of climate change in the presence of internal variability. Chang C.-P., Ghil M., Latif M. and Wallace J.M. (eds). Climate Change: Multidecadal and Beyond (World Scientific), pp:1–29. DOI:10.1142/9789814579933_0001
33. Kay J.E., Deser C., Phillips A., et al. (2015). The community Earth system model (CESM) large ensemble project: A community resource for studying climate change in the presence of internal climate variability. *Bull. Amer. Meteor. Soc.* **96**:1333–1349. DOI:10.1175/BAMS-D-13-00255.1
34. Kalnay E., Kanamitsu M., Kistler R., et al. (1996). The NCEP/NCAR 40-year reanalysis project. *Bull. Amer. Meteor. Soc.* **77**:437–471. DOI:10.1175/1520-0477(1996)077<0437:TNYRP>2.0.CO;2
35. Huang B., Thorne P.W., Banzon V.F., et al. (2017). Extended reconstructed sea surface temperature version 5 (ERSSTv5), upgrades, validations, and intercomparisons. *J. Clim.* **30**:8179–8205. DOI:10.1175/JCLI-D-16-0836.1
36. Adler R.F., Huffman G.J., Chang A., et al. (2003). The version-2 global precipitation climatology project (GPCP) monthly precipitation analysis (1979–present). *J. Hydrometeor.* **4**:1147–1167. DOI:10.1175/1525-7541(2003)004<1147:TVGPCP>2.0.CO;2
37. Eyring V., Bony S., Meehl G.A., et al. (2016). Overview of the coupled model intercomparison project phase 6 (CMIP6) experimental design and organization. *Geosci. Model. Dev.* **9**:1937–1958. DOI:10.5194/gmd-9-1937-2016
38. Cai W.-J., Ng B., Geng T., et al. (2023). Anthropogenic impacts on twentieth-century ENSO variability changes. *Nat. Rev. Earth & Environ.* **4**:407–418. DOI:10.1038/s43017-023-00427-8
39. Austin P.C. and Tu J.V. (2004). Bootstrap methods for developing predictive models. *Am. Stat.* **58**:131–137. DOI:10.1198/0003130043277
40. Jia F., Cai W.-J., Gan B.-L., et al. (2021). Enhanced North Pacific impact on El Niño/Southern Oscillation under greenhouse warming. *Nat. Clim. Chang.* **11**:840–849. DOI:10.1038/s41558-021-01139-x
41. Wang B. and Fan Z. (1999). Choice of South Asian summer monsoon indices. *Bull. Amer. Meteor. Soc.* **80**:629–638. DOI:10.1175/1520-0477(1999)080<0629:COSASM>2.0.CO;2
42. Wu A.M. and Ni Y.Q. (1997). The influence of Tibetan Plateau on the interannual variability of Asian monsoon. *Adv. Atmos. Sci.* **14**:491–504. DOI:10.1007/s00376-997-0067-0
43. Zhang Q.Y., Tao S.Y. and Chen L.T. (2003). The interannual variability of East Asian summer monsoon indices and its association with the pattern of general circulation over East Asia (in Chinese). *Acta Meteor. Sin.* **61**:559–568. DOI:10.11676/qxxb2003.056
44. Ham Y.-G., Kug J.-S., Park J.-Y., et al. (2013). Sea surface temperature in the north tropical Atlantic as a trigger for El Niño/Southern Oscillation events. *Nat. Geosci.* **6**:112–116. DOI:10.1038/ngeo1686
45. Huang B., Schopf P.S. and Shukla J. (2004). Intrinsic ocean–atmosphere variability of the tropical Atlantic Ocean. *J. Clim.* **17**:2058–2077. DOI:10.1175/1520-0442(2004)017<2058:IOVOTT>2.0.CO;2
46. Amaya D.J., DeFlorio M.J., Miller A.J., et al. (2017). WES feedback and the Atlantic Meridional Mode: observations and CMIP5 comparisons. *Clim. Dyn.* **49**:1665–1679. DOI:10.1007/s00382-016-3411-1
47. Cai W.-J., Wu L., Lengaigne M., et al. (2019). Pantropical climate interactions. *Science* **363**:eaav4236. DOI:10.1126/science.aav4236
48. Li X., Xie S.-P., Gille S., et al. (2016). Atlantic induced pan-tropical climate change over the past three decades. *Nat. Clim. Chang.* **6**:275–279. DOI:10.1038/nclimate2840
49. Zhang G.-L., Wang X., Xie Q., et al. (2022). Strengthening impacts of spring sea surface temperature in the north tropical Atlantic on Indian Ocean dipole after the mid-1980s. *Clim. Dyn.* **59**:185–200. DOI:10.1007/s00382-021-06128-6
50. Miyamoto A. and Xie S.-P. (2024). Low cloud–SST variability over the summertime subtropical Northeast Pacific: Role of extratropical atmospheric modes. *J. Clim.* **38**:165–180. DOI:10.1175/JCLI-D-24-0015.1
51. Wang B., Xiang B. and Lee J.-Y. (2013). Subtropical high predictability establishes a promising way for monsoon and tropical storm predictions. *Proc. Natl. Acad. Sci. USA* **110**:2718–2722. DOI:10.1073/pnas.1214626110
52. Tang S., Qiao S., Wang B., et al. (2023). Linkages of unprecedented 2022 Yangtze River Valley heatwaves to Pakistan flood and triple-dip La Niña. *npj Clim. Atmos. Sci.* **6**:8. DOI:10.1038/s41612-023-00386-3
53. Neale R.B., Chen C.-C., Gettelman A., et al. (2010). Description of the NCAR community atmosphere model (CAM 5.0). *NCAR Tech. Note* NCAR/TN-486+STR. DOI: 10.5065/wgtk-4g06.
54. Huang P., Xie S.-P., Hu K.-M., et al. (2013). Patterns of the seasonal response of tropical rainfall to global warming. *Nat. Geosci.* **6**:357–361. DOI:10.1038/ngeo1792
55. Wang G.-J., Cai W.-J., Gan B.-L., et al. (2017). Continued increase of extreme El Nino frequency long after 1.5°C warming stabilization. *Nat. Clim. Chang.* **7**:568–572. DOI:10.1038/nclimate3351
56. Watanabe M., Chikira M., Imada Y., et al. (2011). Convective control of ENSO simulated in MIROC. *J. Clim.* **24**:543–562. DOI:10.1175/2010JCLI3878.1
57. Xiang B., Wang B., Yu W., et al. (2013). How can anomalous western North Pacific subtropical high intensify in late summer. *Geophys. Res. Lett.* **40**:2349–2354. DOI:10.1002/grl.50431
58. Chen S.-F., Chen W., Xie S.-P., et al. (2024). Strengthened impact of boreal winter North Pacific oscillation on ENSO development in warming climate. *npj Clim. Atmos. Sci.* **7**:69. DOI:10.1038/s41612-024-00615-3
59. Yang Y., Wu L.-X., Guo Y., et al. (2021). Greenhouse warming intensifies north tropical Atlantic climate variability. *Sci. Adv.* **7**:eabg9690. DOI:10.1126/sciadv.abg9690
60. Czaja A., Van der Vaart P. and Marshall J. (2002). A diagnostic study of the role of remote forcing in tropical Atlantic variability. *J. Clim.* **15**:3280–3290. DOI:10.1175/1520-0442(2002)015<3280:ADSOTR>2.0.CO;2
61. Wu L. and Liu Z. (2002). Is tropical Atlantic variability driven by the North Atlantic oscillation. *Geophys. Res. Lett.* **29**:1653. DOI:10.1029/2002GL014939
62. Xiang Y.S., Dong L., Song F.F., et al. (2025). Improved simulation of East Asian summer monsoon in the high-resolution CESM1 and its causes. *Adv. Atmos. Sci.* **42**:1110–1126. DOI:10.1007/s00376-024-4229-0

FUNDING AND ACKNOWLEDGMENTS

This study was supported jointly by the National Natural Science Foundation of China (Grants 42475042, 42230605, 42275012, and 42175039), the Yunnan Provincial Science and Technology Department (Grants 202505AB350001 and 202403AP140009), the Natural Science Foundation of Yunnan Province (202302AN360006), and the Youth Program of the Institute of Atmospheric Physics, Chinese Academy of Sciences during the 14th Five-Year Plan Period. We acknowledge the World Climate Research Programme, which, through its Working Group on Coupled Modelling, coordinated and promoted CMIP6. We thank the climate modelling groups for producing and making available their model output, the Earth System Grid Federation (ESGF) for archiving the data and providing access, and the multiple funding agencies who support CMIP6 and ESGF. The funders had no role in study design, data collection and analysis, decision to publish, or preparation of the manuscript.

AUTHOR CONTRIBUTIONS

S. C., W.C., and R.W. designed the research; S.C. analyzed the data and wrote the initial manuscript; S.P.X., C.Z.W. and S.W.Y. contributed to the mechanism analysis; Z.W. performed the numerical experiments; All authors contributed to interpreting results and improving this paper. All authors contributed to the manuscript and approved the final version.

DECLARATION OF INTERESTS

The authors declare no competing interests.

DATA AND CODE AVAILABILITY

The NCEP-NCAR Reanalysis data are derived from https://www.esrl.noaa.gov/psd/data/gridded/data.ncep.reanalysis.derived.html; The ERSSTv5 SST data are derived from https://psl.noaa.gov/data/gridded/data.noaa.ersst.v5.html; The CMIP6 historical and SSP5-8.5 simulation outputs are derived from https://esgf-node.llnl.gov/projects/cmip6/; The GPCP precipitation data are derived from https://psl.noaa.gov/data/gridded/data.gpcp.html. The CAM5 of the CESM model is download at https://www.cesm.ucar.edu/models/cam (last access: 16 September 2025).

SUPPLEMENTAL INFORMATION

It can be found online at https://doi.org/10.59717/j.xinn-geo.2026.100207.